The Self-Assembled Structure of the Diblock Copolymer PCL-*b*-P4VP Transforms Upon Competitive Interactions with Octaphenol Polyhedral Oligomeric Silsesquioxane

Chu-Hua Lu, Shiao-Wei Kuo,* Wen-Teng Chang, Feng-Chih Chang

This paper describes the miscibility and self-assembly, mediated by hydrogen-bonding interactions, of new block copolymer/nanoparticle blends. The morphologies adopted by the immiscible poly[(ε-caprolactone)-*block*-(4-vinyl pyridine)] (PCL-*b*-P4VP) diblock copolymer changes upon increasing the number of competitive hydrogen-bonding interactions after adding increasing amounts of octaphenol polyhedral oligomeric silsesquioxane (OP-POSS). Transmission electron microscopy reveals morphologies that exhibit high degrees of long-range order, such as cylindrical and spherical structures, at relatively low OP-POSS contents, and short-range order or disordered structures at higher OP-POSS contents. Analyses performed using differential scanning calorimetry, wide-angle X-ray diffraction, and FT-IR spectroscopy provide positive evidence that the pyridyl units of the P4VP block are significantly stronger hydrogen-bond acceptors toward the OH group of OP-POSS than are the C=O groups of the PCL block, thereby resulting in excluded and confined PCL phases.

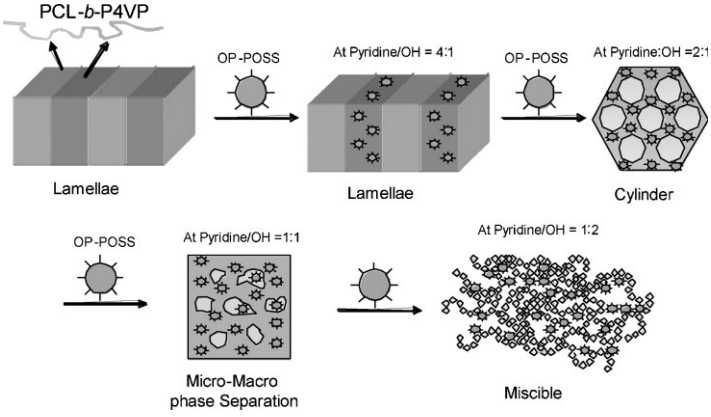

Introduction

Inorganic nanoparticles (NPs) enclosed within self-assembled block copolymer templates provide new opportunities for the development of functional hybrid materials that exhibit enhanced optical, electrical, and mechanical properties.[1–3] For instance, diblock copolymers can form a variety of self-assembled structures that have periodic features on nanometer length scales ranging between 10 and 100 nm.[4,5] Because NPs have sizes between 1 and 10 nm, using diblock copolymers as templates to control the spatial locations of NPs is a natural approach toward the production of hierarchically ordered structures.[6–9] In addition, block copolymer/NP blends are fascinating model systems for studying the mechanisms of structure formation from soft/hard heterogeneous materials.[10]

S.-W. Kuo
Department of Materials and Optoelectronic Science, Center for Nanoscience and Nanotechnology, National Sun Yat-Sen University, Kaohsiung, Taiwan (ROC)
Fax: 886-7-5254099; E-mail: kuosw@faculty.nsysu.edu.tw
C.-H. Lu, W.-T. Chang, F.-C. Chang
Institute of Applied Chemistry, National Chiao-Tung University, Hsin-Chu, Taiwan (ROC)

DOI: 10.1002/marc.200900437

Based on the molecular weight ratios of homopolymer B to block copolymer A-*b*-B ($a = M_{h\text{-}B}/M_{b\text{-}B}$), A-*b*-B block copolymer/B homopolymer blending systems can be divided into three categories: completely phase separated systems ($a >> 1$), "dry brush" blend systems ($a =$ ca. 1), and "wet brush" blend systems ($a < 1$).[11] In the wet brush system, the added homopolymer B is uniformly dissolved in the block copolymer B microdomains and, thereby, changes the micro-domain size or even the morphology. This behavior is similar to that found in block copolymer/NP systems.[12] Wei et al. reported that simple cubic structures were obtained from composites of poly[styrene-*block*-(ethylene oxide)] (PS-*b*-PEO) and CdS NPs when using an originally hexagonally packed cylindrical PS-*b*-PEO structure and CdS NPs having surfaces modified with ethanol functional groups. These modified CdS NPs tether selectively to PEO chains through hydrogen bonding and disperse well within the PEO domains of PS-*b*-PEO.[13] The NP-induced transformations of other self-assembled A-*b*-B structures have been investigated in several previous studies,[14–20] essentially all of which involved systems in which the NPs were immiscible with block A but interacted favorably with block B.

In this communication, we report a new system in which poly[(ε-caprolactone)-*block*-(4-vinyl pyridine)] (PCL-*b*-P4VP) transforms from a lamellar structure to a hexagonally packed cylinder structure and then to a miscible phase upon increasing the content of octaphenol polyhedral oligomeric silsesquioxane (OP-POSS) NPs. In this system, the OP-POSS NPs (component C) are miscible with both blocks A and B, but the hydrogen bonds between segments B and C are stronger than those between segments A and C ($\chi_{BC} >> \chi_{AC}$). POSS compounds, unique cage-like structures that possess nanometer-scale dimensions, are of particular interest in preparing hybrid materials. These inorganic/organic hybrid architectures contain an inner inorganic framework composed of silicon and oxygen [$(SiO_{1.5})_x$] surrounded by organic substituents.[21–24] In previous studies, we developed a simple two-step synthesis of OP-POSS through hydrosilylation of 4-acetoxystyrene with octasilane POSS ($Q_8M_8^H$), and subsequent hydrolysis of the acetoxy units.[25–28] OP-POSS possesses eight phenolic groups, which form hydrogen bonds with several hydrogen-bonded acceptor groups (e.g., pyridine, C=O, ether, and ester units). The hydrogen-bonding interactions in phenol/P4VP blends ($K_A = 598$)[29] are significantly stronger than those in phenol/PCL blends ($K_A = 90$),[30,31] based on the Painter–Coleman association model (PCAM).[32] PCL and P4VP form an immiscible blend. In this study, we used differential scanning calorimetry (DSC), wide-angle X-ray diffraction (WAXD), transmission electron microscopy (TEM), small-angle X-ray scattering (SAXS), and FT-IR spectroscopy to characterize the self-assembly and competitive specific interactions in PCL-*b*-P4VP/OP-POSS blends.

Experimental Part

Materials

The poly[(ε-caprolactone)-*block*-(4-vinyl pyridine)] (PCL_{175}-*b*-$P4VP_{117}$) copolymer was synthesized through ring-opening polymerization of ε-caprolactone followed by free radical polymerization of 4-vinyl pyridine; details of the synthetic route and characterization are available elsewhere.[33–35] OP-POSS was synthesized through a simple two-step synthesis: hydrosilylation of 4-acetoxystyrene with octasilane POSS ($Q_8M_8^H$) and subsequent hydrolysis of the acetoxy units.[25–28]

Block Copolymer/NP Preparation

Blend samples that contained various molar fractions of PCL-*b*-P4VP and OP-POSS were prepared through solution casting. A *N*,*N*-dimethylformamide (DMF) solution that contained 5 wt.-% of the blend was stirred for 8–10 h and then cast on a Teflon dish. The solvent was evaporated slowly at 80 °C for 1 d and then the sample was dried in a vacuum oven at 120 °C for 14 d.

Characterization

Thermal analysis was performed using a DSC instrument (TA Instruments Q-20). For non-isothermal crystallization experiments, the sample was first annealed at 210 °C for 10 min and then cooled to −90 °C at 5 °C · min^{-1} to record the crystallization exotherm. The glass transition temperature (T_g) was taken as the midpoint of the heat capacity transition between the upper and lower points of deviation from the extrapolated glass and liquid lines recorded at a scan rate of 20 °C · min^{-1} over the temperature range from −90 to +250 °C. TEM analysis was performed using a Hitachi H-7100 electron microscope operated at 100 kV. Ultrathin sections of the samples were prepared using a Leica Ultracut S microtome equipped with a diamond knife. WAXD measurements were performed using a Bruker Nanostar U system, with an incident X-ray wavelength (λ) of 0.1542 nm. SAXS experiments were performed using the SAXS instrument at the BL17B3 beamline of the National Synchrotron Radiation Research Center (NSRRC), Taiwan. FT-IR spectra were measured using the KBr disk method and a Nicolet Avatar 320 FTIR spectrometer, 32 scans were collected at a resolution of 1 cm^{-1}. A DMF solution that contained the sample was cast onto a KBr disk and then dried under conditions similar to those used for the bulk preparation.

Results and Discussion

Figure 1a displays conventional second-run DSC thermograms, obtained with a heating rate of 20 °C · min^{-1}, of PCL-*b*-P4VP/OP-POSS blends of various compositions. The pure PCL-*b*-P4VP block copolymer exhibited two T_gs and a melting temperature (T_m) because of the immiscibility of the PCL and P4VP segments. The values of T_g of the PCL and P4VP blocks and OP-POSS were ca. −60, 150, and 18 °C, respectively. The value of T_m of the PCL block was ca. 55 °C.

Macromolecular Journals
DOI: 10.1002/marc.200900437

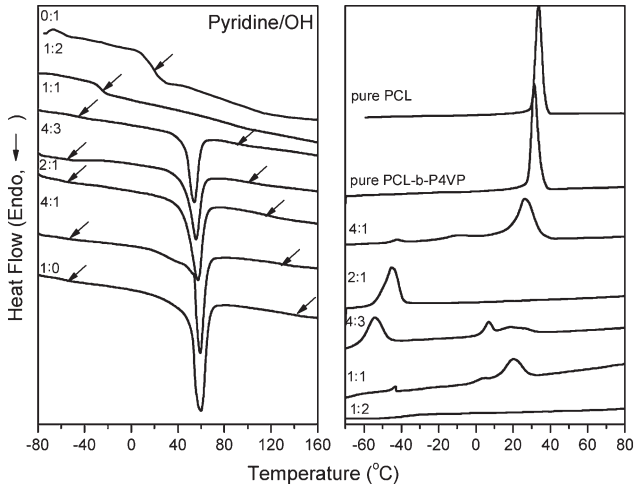

Figure 1. DSC thermograms of PCL-*b*-P4VP/OP-POSS blends during a) heating and b) cooling.

The value of T_g of the amorphous P4VP (150 °C) was substantially higher than the melting point of the PCL crystallites, which tend to induce hard confinement.[36–38] Consequently, this well-defined system generated strong segregation limits [high $(\chi N)_{Tc}$ value] for polymer crystallization under vitrified nanometer-scale confinement.[39] The value of T_g of the P4VP block decreased, whereas that of the PCL block remained unchanged, upon blending the PCL-*b*-P4VP block copolymer with increasing amounts of OP-POSS at lower content. Therefore, we suspected that the added OP-POSS interacted preferentially with P4VP through hydrogen bonding. In addition, the melting peak of the crystalline PCL gradually disappeared with the increase of OP-POSS content, which indicates hydrogen-bonding interactions between the OP-POSS and PCL. In addition, the melting peak disappeared completely when the molar ratio of pyridyl to OH was 1:2. At this ratio, the PCL-*b*-P4VP/OP-POSS blends exhibited only one glass transition temperature, which suggests that the blend had become miscible. Eventually, OP-POSS acted as a common solvent for both PCL and P4VP, thereby inducing the blends to become totally miscible (disordered structure).

Figure 1b presents DSC cooling curves for the PCL-*b*-P4VP/OP-POSS blends obtained at a fixed cooling rate of 5 °C · min^{-1}. The freezing temperature (T_f) is defined as the peak temperature of the crystallization exotherm. A higher value of T_f corresponds to a faster crystallization rate. The freezing temperature is generally associated with non-isothermal crystallization under a fixed cooling rate; it is distinctly correlated to the microdomain structure.[40–46] Although we observed a single exotherm at lower OP-POSS contents (pyridyl/OH molar ratios from 1:0 to 4:1), peculiar crystallization behavior (second exotherm) occurred at higher OP-POSS contents (pyridyl/OH molar ratios from 2:1 to 4:3). This second exotherm at lower values of T_f was not present for the PCL homopolymer, but appeared at a much larger under-cooling temperature. Because of the lower PCL content, the PCL phase formed a regular disperse phase, the average size of which was very small and the number of particles was significantly greater than the number of active heterogeneities usually present in this blend — so-called "hard confinement". Therefore, we observed only one exotherm when the pyridyl/OH molar ratio was 2:1. Upon further increasing the OP-POSS content (pyridyl/OH molar ratios from 4:3 to 1:2), the OP-POSS began to interact with PCL, as evidenced through FT-IR spectroscopic analyses (see below). Therefore, the self-assembled structure changed to a short-range-ordered or miscible structure because PCL confinement disappeared as a result of hydrogen bonding with OP-POSS. Crystallization may occur with more than one exotherm — a phenomenon known as fractionated crystallization.[47,48] In addition, this block copolymer/NP blend featured only one melting temperature in Figure 1a. This behavior can be understood by considering that the first crystallization process (exotherm I) was produced by heterogeneous crystallization (continuous domains, in which case crystal growth could propagate throughout the sample), whereas the second exotherm was produced by homogeneous nucleation (from these non-connecting PCL domains of the OP-POSS/P4VP mixed phase), as indicated in Figure 2c and 2d. A similar phenomenon was reported by Chen et al.,[40,41] who found that when strongly segregated diblock systems were subjected to a fixed cooling rate, the freezing temperature-associated non-isothermal crystallization exhibited a distinct correlation with the microdomain structure and the value of T_f dropped abruptly as the melt morphology shifted from extended lamellae to dispersed cylinders. A second drop in the value of T_f was also observed as the morphology further transformed into spheres. The degree of supercooling ($\Delta T = T_m^0 - T_f$, $T_m^0 = 75$ °C)[49] required to initiate crystallization in the lamellar microdomains ($\Delta T = 50$ °C) was comparable with that associated with the PCL homopolymer ($\Delta T = 42$ °C). Exceedingly large undercoolings are required for crystallization in cylinders ($\Delta T = 125$ °C). The crystallization kinetics exhibited distinct transition at the compositions that corresponded to the morphological transformation, which indicates the feasibility of exploiting the micro-domain pattern by manipulating the crystallization kinetics of the block chains. Figure 1b reveals that pure PCL-*b*-P4VP exhibited a freezing temperature at ca. 30 °C. We would expect a lamellar structure in these pure diblock copolymers, as indicated in the TEM image in Figure 2a. The freezing temperature decreased slightly to 25 °C at a pyridyl/OH molar ratio of 4:1. This system also featured a lamellar structure (Figure 2b). In contrast, the freezing temperature decreased significantly (to −45 °C) at a pyridyl/OH molar ratio of 2:1 because the freezing temperature shifted from lamellae ($T_f = 25$–35 °C) to

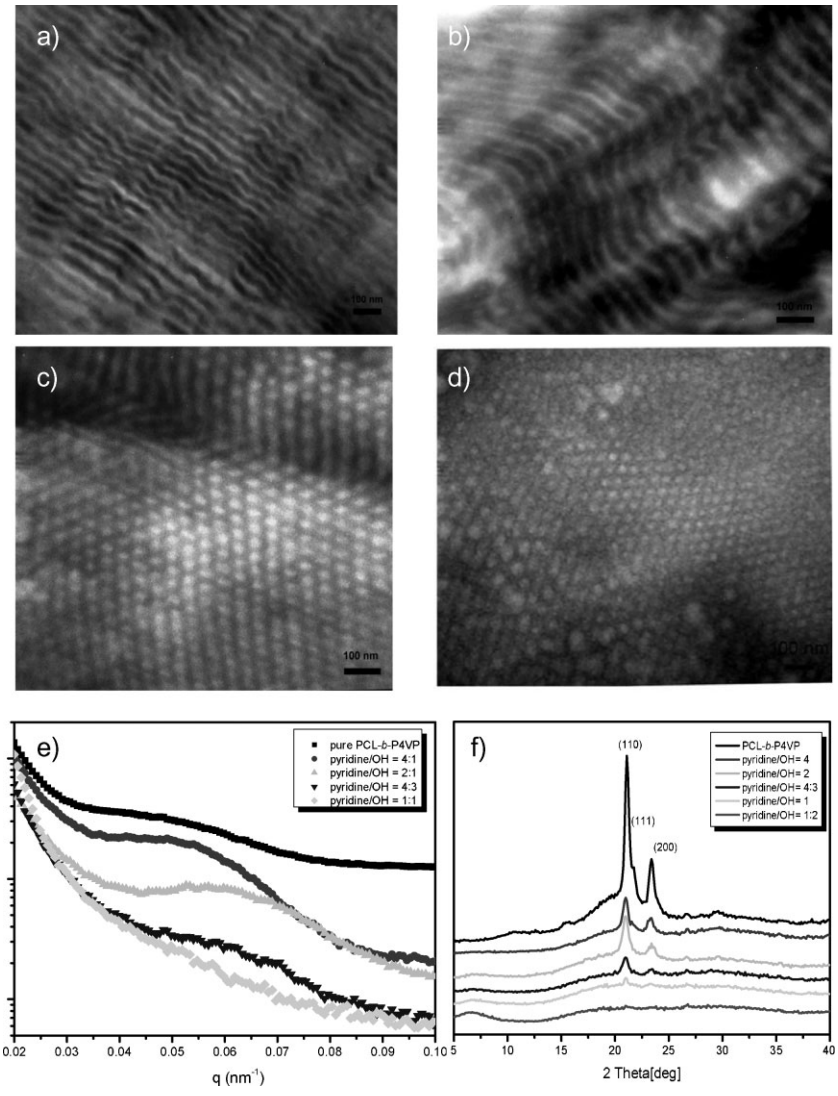

Figure 2. TEM images of a) the pure PCL-*b*-P4VP diblock copolymer, stained with I_2, and the PCL-*b*-P4VPOP-POSS blends at pyridyl/OH molar ratios of b) 4:1, c) 2:1, and d) 4:3, without staining. e) SAXS and f) WAXD data of the PCL-*b*-P4VP/OP-POSS blends.

cylinders ($T_f = -45$ to -50 °C). Therefore, we expected that a pyridyl/OH molar ratio of 2:1 would provide the cylinder structure, as indicated in Figure 2c. A further increase in the OP-POSS content (pyridyl/OH ratio of 4:3) resulted in two exotherms appearing because of 'fractionated crystallization', where the long-range cylinder structure transformed into a short-range-ordered structure (Figure 2d). In other words, the self-assembled morphology of PCL-*b*-P4VP was transformed after blending with OP-POSS at pyridyl/OH molar ratios from 2:1 to 1:1 because the added OP-POSS formed hydrogen bonds preferentially with the P4VP block and the PCL block was confined within the OP-POSS/P4VP phase. The crystalline PCL was destroyed, however, and no crystallization exotherm appeared when the pyridyl/OH molar ratio was 1:2. Thus, the OP-POSS content in the blend plays an important role in affecting the crystallization behavior and the morphological changes because of nanostructural confinement.[40]

Figure 2e displays SAXS profiles of PCL-*b*-P4VP/OP-POSS blends at room temperature, where the self-assembled structures overlap with the long-period structure of crystalline PCL. At lower OP-POSS contents, the broad first-order scattering peak had a Bragg spacing of ca. 10.2–12.5 nm, which corresponds to the long-period structure of crystalline PCL. The blends at higher OP-POSS contents exhibited broader peaks that correspond to disordered amorphous structures, an indication that the long-period crystalline structure was absent. The reduction in the *d*-spacing due to the diluting interaction parameter (χN) reduces, as χ is reduced because of the solvent (P4VP/OP-POSS) and the reduction in the SAXS contrast as the solvent does not exclusively partition to one phase.

We observed similar results in the WAXD analyses presented in Figure 2f, where the crystalline PCL exhibited two distinct diffraction peaks for all blends at values of 2θ of 21.5 and 23.8° for the (110) and (200) reflections, respectively, which corresponds to orthorhombic packing as the perfect crystallographic orientation of its crystalline structure.[46] The appearance of these diffraction peaks of crystalline PCL in blends was a result of immiscibility between the PCL and P4VP blocks. The intensities of these crystallization peaks decreased gradually upon increasing the OP-POSS content from a pyridyl/OH molar ratio of 4:1 to 1:1. Further increasing the OP-POSS content to a pyridyl/OH molar ratio of 1:2 resulted in the disappearance of these crystallization peaks and the appearance of amorphous halos, because a large number of the OH groups of OP-POSS formed hydrogen bonds with the pyridyl groups of P4VP and the C=O groups of PCL. In other words, the blend became miscible and the crystalline structure of the PCL was destroyed, consistent with our observations from FT-IR spectroscopic analysis. As mentioned above in our discussions of the DSC, SAXS, and TEM analyses, the hydrogen-bond strength in OP-POSS/P4VP blends is stronger than that in OP-POSS/PCL systems. Further increasing the OP-POSS content allows the excess OP-POSS to hydrogen bond with both the P4VP and PCL blocks. Therefore, at higher OP-POSS contents, the blends

Macromol. Rapid Commun. **2009**, *30*, 2121–2127

Macromolecular Journals
DOI: 10.1002/marc.200900437

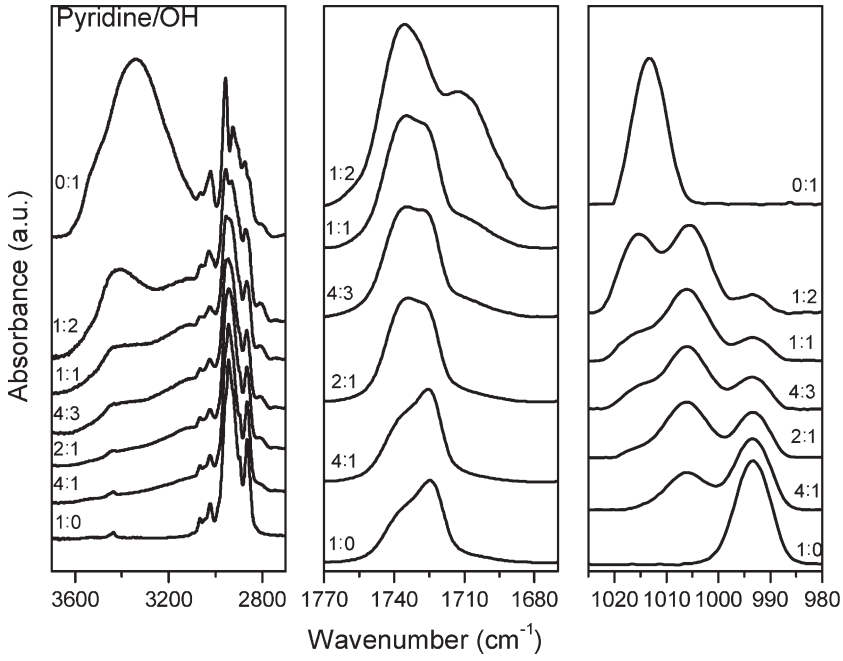

Figure 3. FT-IR spectra of the PCL-*b*-P4VPOP-POSS blends, recorded at room temperature, displaying the a) OH stretching, b) C=O, and c) pyridyl regions.

were miscible and OP-POSS acted as a common solvent for both blocks. We used FTIR spectroscopy to provide evidence to support this claim.

Hydrogen-bonding interactions influence several regions within the FT-IR spectra of the PCL-*b*-P4VP/OP-POSS blends. Figure 3a displays the OH stretching region of various PCL-*b*-P4VP/OP-POSS blends. Pure OP-POSS provided two unresolved bands in the OH stretching region that corresponded to the free OH groups at 3 525 cm^{-1} and a very broad band centered at 3 350 cm^{-1} from the absorption of hydrogen-bonded OH groups (self-association). The signals for the OH groups shifted to a lower wavenumber when a high content of P4VP was present in the blend (lower OP-POSS content), which implies that the OH groups of OP-POSS interacted preferably with the pyridyl groups of P4VP. Therefore, we assign the band at 3 125 cm^{-1} to the OH groups hydrogen bonded to the pyridyl units because a relatively small number of the OH groups interacted completely with pyridyl groups of the P4VP blocks to form hydrogen bonds. Meanwhile, the peak frequency of the broad band shifted to a higher wavenumber upon increasing the OP-POSS content, which reflected the new distribution of non-covalent interactions resulting from competition between OH···OH hydrogen bonds of OP-POSS units and OH···O=C hydrogen bonds between OP-POSS and PCL blocks (3 430 cm^{-1}). Moskala and co-workers used the frequency difference between the hydrogen-bonded OH absorption and the free absorption ($\Delta\nu$) to roughly estimate the average hydrogen-bond strength.[50] In this respect, the hydrogen-bonding interactions between the OP-POSS OH and P4VP pyridyl groups ($\Delta\nu = 400\ cm^{-1}$) were substantially stronger than those between the OP-POSS OH and PCL C=O groups ($\Delta\nu = 95\ cm^{-1}$), consistent with the predictions of the PCAM. According to the PCAM, the inter-association equilibrium constant of the OP-POSS/P4VP blend ($K_A = 598$) would be significantly greater than that of the OP-POSS/PCL blend ($K_A = 90$), which implies that hydrogen-bond formation between OP-POSS and the P4VP blocks should predominate over that between OP-POSS and the PCL blocks in these PCL-*b*-P4VP/OP-POSS blends.

The C=O groups of the PCL blocks are sensitive to hydrogen-bonding interactions. The peaks at 1 735, 1 724, and 1 710 cm^{-1} in Figure 3b correspond to the free C=O, the crystalline conformation, and hydrogen-bonded C=O groups, respectively. The hydrogen-bonded C=O band of PCL at 1 710 cm^{-1} appeared in the spectra of the blends containing OP-POSS at pyridyl/OH molar ratios ranging from 4:3 to 1:2, which indicated that the OP-POSS OH groups began to interact with the PCL C=O groups in these blends. As expected, a higher content of OP-POSS units resulted in a higher number of hydrogen-bonded C=O groups. In addition, the band at 993 cm^{-1} could also be used to analyze the hydrogen-bonding interactions between the OH groups of PVPh and the pyridyl groups of P4VP. Figure 3c displays scale-expanded (980–1 025 cm^{-1}) FT-IR spectra of PCL-*b*-P4VP and the PCL-*b*-P4VP/OP-POSS blends. Pure PCL-*b*-P4VP provided a characteristic band at 993 cm^{-1}, which corresponded to the pure pyridyl ring absorption of the P4VP block. Pure OP-POSS does not absorb at 993 cm^{-1}, but it does provide a band at 1 013 cm^{-1}. These two bands are well resolved without overlapping. Hydrogen bonding between OP-POSS and the P4VP blocks resulted in a new band at 1 005 cm^{-1}, which we assign to the hydrogen-bonded pyridyl rings.[9] It is difficult to calculate the quantitative fraction of hydrogen bonds because of the presence of three bands in this region. As a result, we performed digital subtraction of the pure PVPh peak at 1 013 cm^{-1}, based on the mole fraction of the PVPh in these blends. The Gaussian function was used for curve fitting of the stretching frequencies of the free and hydrogen-bonded C=O groups of PCL at 1 735 and 1 710 cm^{-1}, respectively, and of the pyridyl bands of P4VP at 993 and 1 005 cm^{-1}, respectively. To obtain the true fraction of hydrogen-bonded groups required us to know the absorptivity ratio for the hydrogen-bonded and

Table 1. Curve fitting of hydrogen-bonded C=O and pyridyl groups in PCL-*b*-P4VP/OP-POSS blends.

Composition	Crystalline C=O			Free C=O			H-bonded C=O			f_b
	ν	$W_{1/2}$	A_c	ν	$W_{1/2}$	A_f	ν	$W_{1/2}$	A_b	
PCL-*b*-P4VP	1 725	14	45.80	1 737	19	54.20	–	–	–	–
pyridyl/OH = 4/1	1 725	14	46.36	1 737	19	53.64	–	–	–	–
pyridyl/OH = 2/1	1 725	14	34.00	1 737	19	66.00	–	–	–	–
pyridyl/OH = 4/3	1 725	14	24.77	1 737	19	60.49	1 711	27	14.73	13.97
pyridyl/OH = 1/1	1 725	14	23.12	1 737	19	56.94	1 711	27	19.94	18.93
pyridyl/OH = 1/2	–	–	–	1 736	19	54.84	1 711	26	45.16	35.44
Composition	**Free pyridyl**			**H-bonded pyridyl**			**Phenol group**			f_b
	ν	$W_{1/2}$	A_f	ν	$W_{1/2}$	A_H	ν	$W_{1/2}$	A_P	
PCL-*b*-P4VP	993	8	100.0	–	–	–	–	–	–	–
pyridyl/OH = 4/1	993	8	68.07	1 006	9	31.93	–	–	–	31.93
pyridyl/OH = 2/1	993	7	38.35	1 006	9	56.90	1 015	6	4.75	59.74
pyridyl/OH = 4/3	993	7	26.99	1 006	9	61.55	1 016	6	11.46	69.51
pyridyl/OH = 1/1	993	7	20.36	1 006	9	66.38	1 015	6	13.26	76.53
pyridyl/OH = 1/2	993	7	7.27	1 006	9	59.59	1 016	6	33.14	89.13

free groups; we employed values of α_{HB}/α_F of 1.5 for the C=O groups of PCL and 1.0 for the pyridyl groups of P4VP.[51,52] Table 1 summarizes the fractions of hydrogen-bonded C=O and pyridyl groups in the PCL-*b*-P4VP/OP-POSS blends. The OP-POSS OH groups formed hydrogen bonds with both the P4VP and PCL blocks when the pyridyl/OH molar ratio was greater than 4:3. In other words, the OH groups of OP-POSS formed hydrogen bonds preferentially with the pyridyl groups of P4VP when the pyridyl/OH molar ratio was less than 4:3.

Scheme 1 plots the morphological transformation that occurred upon increasing the OP-POSS content. Long-range-ordered nanostructures existed in the PCL-*b*-P4VP/OP-POSS blend at low OP-POSS contents (lamellar and cylinder structures at pyridyl/OH molar ratios of greater than 4:1 and 2:1, respectively), only short-range-ordered nanostructures existed at relatively higher OP-POSS contents (pyridyl/OH molar ratios ranging from 4:3 to 1:1), and disordered structures existed at high OP-POSS contents (pyridyl/OH molar ratios of less than 1:2).

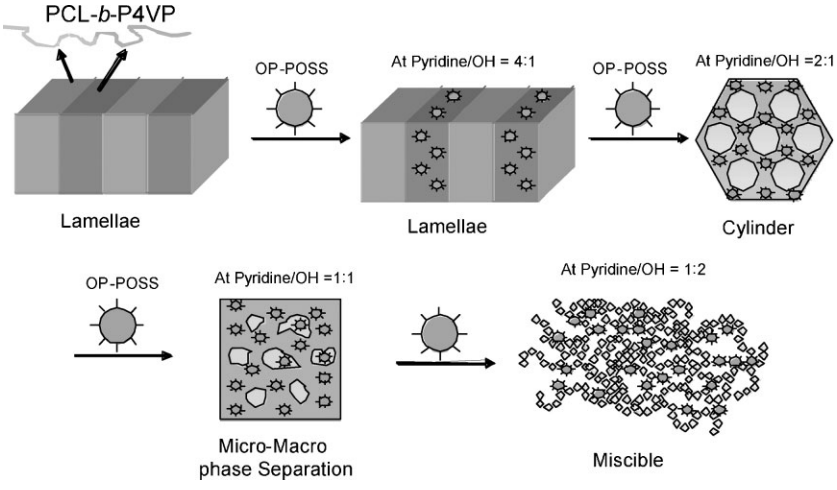

Scheme 1. Morphological changes in PCL-*b*-P4VP/OP-POSS blends upon increasing the OP-POSS content.

Conclusion

We have used DSC, WAXD, TEM, SAXS, and FT-IR spectroscopy to investigate, in detail, the miscibility, phase behavior, and hydrogen-bonding interactions of novel block copolymer/OP-POSS blends. DSC revealed that the structural transition of the PCL block occurred as a result of changing the value of T_f of PCL. TEM images indicated that different compositions of the PCL-*b*-P4VP/OP-POSS blends formed different microphase-separated structures through the effects of hydrogen bonds, even though PCL-*b*-P4VP is an immiscible block copolymer. FT-IR spectra provided evidence that the

Macromol. Rapid Commun. **2009**, *30*, 2121–2127

DOI: 10.1002/marc.200900437

pyridyl groups of P4VP are significantly stronger hydrogen-bond acceptors than the C=O groups of PCL, and that OP-POSS interacts with the P4VP block preferentially in PCL-*b*-P4VP/OP-POSS blends because of these stronger hydrogen-bonding interactions. As a result, we obtained different self-assembled structures in the PCL-*b*-P4VP/OP-POSS blends upon varying the OP-POSS contents.

Acknowledgements: This study was supported financially by the *National Science Council*, Taiwan, Republic of China, under contracts NSC 97-2221-E-110-013-MY3 and NSC 97-2120-M-009-003.

Received: June 22, 2009; Published online: September 11, 2009; DOI: 10.1002/marc.200900437

Keywords: block copolymers; hydrogen bonding; nanoparticles; self assembly

[1] M. R. Bockstaller, R. A. Mickiewicz, E. L. Thomas, *Adv. Mater.* **2005**, *17*, 1331.
[2] M. Lazzari, M. A. Lopez-Quintela, *Adv. Mater.* **2003**, *15*, 1583.
[3] C. Burda, X. B. Chen, R. Narayanan, M. A. El-Sayed, *Chem. Rev.* **2005**, *105*, 1025.
[4] L. Zhu, S. Z. D. Cheng, P. Huang, Q. Ge, R. P. Quirk, E. L. Thomas, B. Lotz, B. S. Hsiao, F. Yeh, L. Liu, *Adv. Mater.* **2002**, *14*, 31.
[5] J. Z. Zhang, *Acc. Chem. Res.* **1997**, *30*, 423.
[6] P. Simon, U. Schwarz, R. Kniep, *J. Mater. Chem.* **2005**, *15*, 4992.
[7] M. J. Birnkrant, C. Y. Li, L. V. Natarajan, V. P. Tondiglia, R. L. Sutherland, P. F. Lloyd, T. J. Bunning, *Nano Lett.* **2007**, *7*, 3128.
[8] H. D. Wagner, *Nat. Nanotechnol.* **2007**, *2*, 742.
[9] R. Vaia, J. Baur, *Science* **2008**, *319*, 420.
[10] M. R. Bockstaller, Y. Lapetnikov, S. Margel, E. L. Thomas, *J. Am. Chem. Soc.* **2003**, *125*, 5276.
[11] J. J. Chiu, B. J. Kim, E. J. Kramer, D. J. Pine, *J. Am. Chem. Soc.* **2005**, *127*, 5036.
[12] U. S. Jeng, Y. S. Sun, H. J. Lee, C. H. Hsu, K. S. Liang, S. W. Yeh, K. H. Wei, *Macromolecules* **2004**, *37*, 4617.
[13] H. Tanaka, H. Hasegawa, T. Hashimoto, *Macromolecules* **1991**, *24*, 240.
[14] S. W. Yeh, K. H. Wei, Y. S. Sun, U. S. Jeng, K. S. Liang, *Macromolecules* **2003**, *36*, 7903.
[15] S. W. Yeh, K. H. Wei, Y. S. Sun, U. S. Jeng, K. S. Liang, *Macromolecules* **2005**, *38*, 6559.
[16] B. Lee, C. T. Lo, S. Seifert, N. L. D. Rago, R. E. Winans, P. Thiyagarajan, *Macromolecules* **2007**, *40*, 4235.
[17] J. Listak, M. R. Bockstaller, *Macromolecules* **2006**, *39*, 5820.
[18] C. Xu, K. Ohno, V. Ladmiral, D. E. Milkie, J. M. Kikkawa, R. J. Composto, T. Lookman, *Macromolecules* **2009**, *42*, 1219.
[19] R. B. Thompson, K. Rasmussen, T. Lookman, *Nano Lett.* **2004**, *4*, 2455.
[20] S. W. Yeh, Y. T. Chang, C. H. Chou, K. H. Wei, *Macromol. Rapid Commun.* **2004**, *25*, 1680.
[21] H. Xu, S. W. Kuo, J. S. Lee, F. C. Chang, *Macromolecules* **2002**, *35*, 8788.
[22] S. H. Phillips, T. S. Haddad, S. J. Tomczak, *Curr. Opin. Solid State Mater. Sci.* **2004**, *8*, 21.
[23] S. W. Kuo, H. F. Lee, W. J. Huang, K. U. Jeong, F. C. Chang, *Macromolecules* **2009**, *42*, 1619.
[24] S. W. Kuo, Y. C. Wu, C. H. Lu, F. C. Chang, *J. Polym. Sci., Part B: Polym. Phys.* **2009**, *17*, 811.
[25] Y. J. Yen, S. W. Kuo, C. F. Huang, J. K. Chen, F. C. Chang, *J. Phys. Chem. B* **2008**, *112*, 10821.
[26] Y. C. Sheen, C. H. Lu, C. F. Huang, S. W. Kuo, F. C. Chang, *Polymer* **2008**, *49*, 4017.
[27] H. C. Lin, S. W. Kuo, C. F. Huang, F. C. Chang, *Macromol. Rapid Commun.* **2006**, *27*, 537.
[28] S. W. Kuo, H. C. Lin, W. J. Huang, C. F. Huang, F. C. Chang, *J. Polym. Sci., Part B: Polym. Phys.* **2006**, *44*, 673.
[29] S. W. Kuo, P. H. Tung, F. C. Chang, *Macromolecules* **2006**, *39*, 9388.
[30] S. W. Kuo, C. F. Huang, C. H. Lu, F. C. Chang, *Macromol. Chem. Phys.* **2006**, *207*, 2006.
[31] S. W. Kuo, S. C. Chan, F. C. Chang, *Macromolecules* **2006**, *36*, 6653.
[32] M. M. Coleman, P. C. Painter, *"Miscible Polymer Blends — Background and Guide for Calculations and Design"*, DEStech Publications, Inc., Lancaster, PA 2006.
[33] C. H. Lu, C. F. Huang, S. W. Kuo, F. C. Chang, *Macromolecules* **2009**, *42*, 1067.
[34] S. C. Chan, S. W. Kuo, C. H. Lu, H. F. Lee, F. C. Chang, *Polymer* **2007**, *48*, 5059.
[35] W. C. Chen, S. W. Kuo, C. H. Lu, F. C. Chang, *Macromolecules* **2009**, *42*, 3580.
[36] P. Huang, L. Zhu, Y. Gau, Q. Ge, A. J. Jing, W. Y. Chen, R. P. Quirk, S. Z. D. Cheng, E. L. Thomas, B. Lotz, B. S. Hsiao, C. A. Avilaorta, I. Sics, *Macromolecules* **2004**, *37*, 3689.
[37] L. Zhu, S. Z. D. Cheng, B. H. Callhoun, Q. Ge, R. P. Quirk, E. L. Thomas, B. Lotz, B. S. Hsiao, F. Yeh, L. Liu, *Macromolecules* **2001**, *34*, 1244.
[38] L. Zhu, S. Z. D. Cheng, B. H. Calhoun, Q. Ge, R. P. Quirk, E. L. Thomas, B. S. Hsiao, F. Yeh, B. Lotz, *J. Am. Chem. Soc.* **2000**, *122*, 5957.
[39] Y. S. Sun, T. M. Chung, Y. J. Li, R. M. Ho, B. T. Ko, U. S. Jeng, B. Lotz, *Macromolecules* **2006**, *39*, 5782.
[40] H. L. Chen, S. C. Hsiao, T. L. Lin, K. Yamauchi, H. Hasegawa, T. Hashimoto, *Macromolecules* **2001**, *34*, 671.
[41] H. L. Chen, J. C. Wu, T. L. Lin, J. S. Lin, *Macromolecules* **2001**, *34*, 6936.
[42] Y. L. Loo, R. A. Register, A. J. Ryan, G. T. Dee, *Macromolecules* **2001**, *34*, 8968.
[43] H. L. Chen, S. Y. Lin, Y. Y. Huang, F. C. Chiu, W. Liou, J. S. Lin, *Macromolecules* **2002**, *35*, 9434.
[44] J. T. Xu, S. C. Turners, J. P. A. Fairclough, S. M. Mai, A. J. Ryan, C. Chaibundit, C. Booth, *Macromolecules* **2002**, *35*, 3614.
[45] J. Y. Hsu, I. F. Hsieh, B. Nandan, F. C. Chiu, J. H. Chen, U. S. Jeng, H. L. Chen, *Macromolecules* **2007**, *40*, 5014.
[46] C. L. He, J. R. Sun, M. X. Deng, X. S. Chen, X. B. Jing, *Biomacromolecules* **2004**, *5*, 2042.
[47] V. Balsamo, F. von Gyldenfeldt, R. Stadler, *Macromolecules* **1999**, *32*, 1226.
[48] V. Balsamo, F. von Gyldenfeldt, R. Stadler, *Macromol. Chem. Phys.* **1996**, *197*, 33.
[49] J. Sun, X. Chen, C. He, X. Jing, *Macromolecules* **2006**, *39*, 3717.
[50] E. J. Moskala, D. F. Varnell, M. M. Coleman, *Polymer* **1985**, *26*, 228.
[51] S. W. Kuo, P. H. Tung, F. C. Chang, *Macromolecules* **2006**, *39*, 9388.
[52] L. C. Cesteros, E. Meaurio, I. Katime, *Macromolecules* **1993**, *26*, 2323.